Karlsruhe Institute of Technology

Damage in silica by hydroxyl generation described by Wang's theoretical data

T. Fett, G. Schell

KIT SCIENTIFIC WORKING PAPERS 85

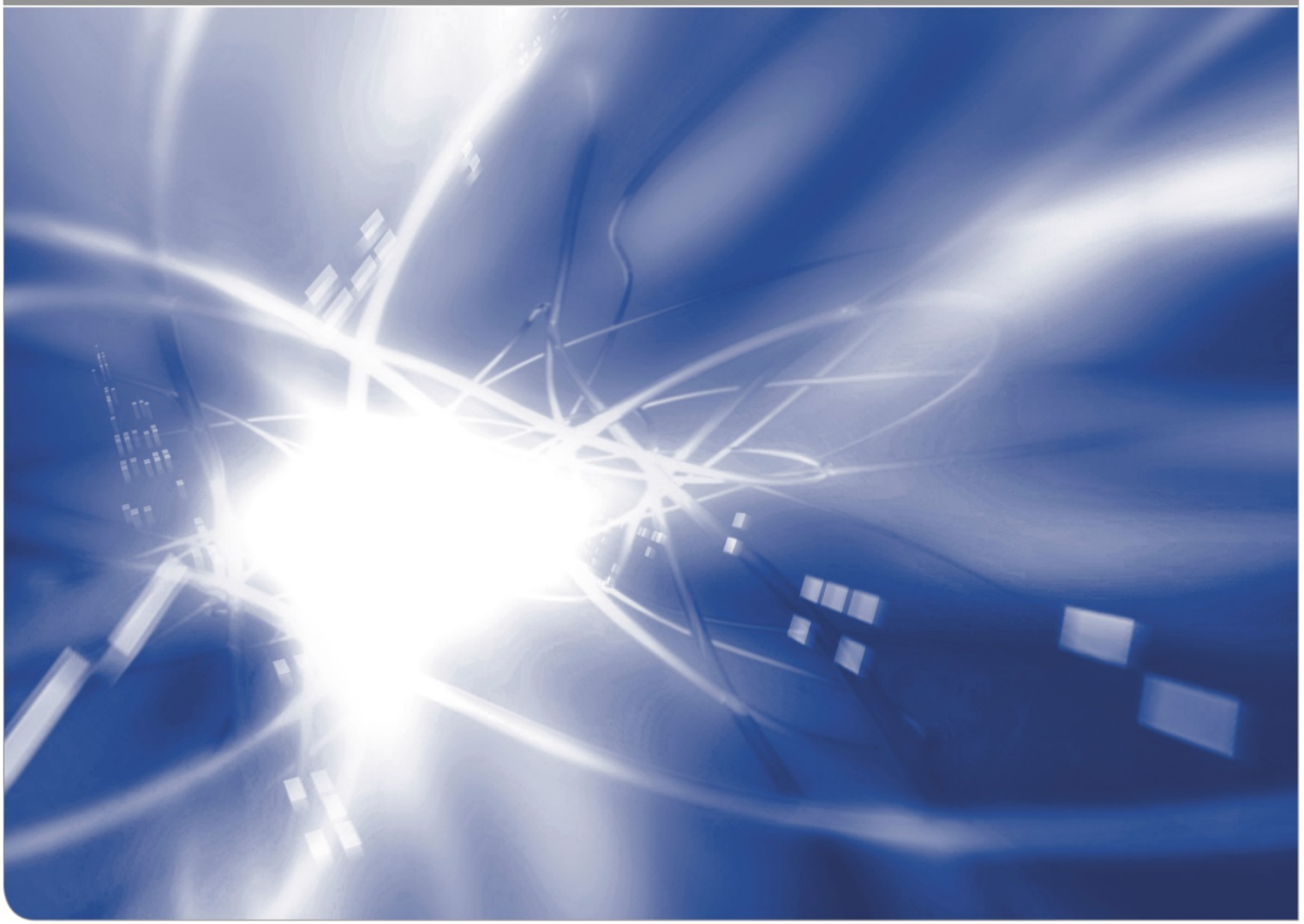

Institut für Angewandte Materialien, Karlsruher Institut für Technologie (KIT)

Impressum

Karlsruher Institut für Technologie (KIT)
www.kit.edu

2018

ISSN: 2194-1629

Abstract

Water diffusion into silica glass results in a thin zone near the surface of the glass. In this zone the water reacts with the SiO_2 structure and "damages" the originally intact SiO_2 rings. The consequence is a reduced Young's module. This effect can be described by use of continuum damage mechanics according to Kachanov and Lemaitre.

In this report the dependency between hydroxyl concentration and damage will be described for large water concentrations by using the Wang-model. In addition the implications on strength of pre-damaged materials, deformation behavior and crack-tip stress intensity factor are addressed.

Contents

1 Damage by hydroxyl generation

When a hydroxyl has been formed, the initial silica ring is broken and the mechanical cohesion is weakened as is illustrated in Fig. 1. Such "defects" in the glass structure can be treated by using the damage variable D of continuum damage mechanics (Kachanov [1], Lemaitre [2]). This parameter is proportional to the density of micro-defects.

According to the postulate of strain equivalence by Lemaitre [3], the effective elastic modulus, E_D, decreases with increasing damage

$$E_D = E_0(1-D) \tag{1.1}$$

where E_0 is the modulus of virgin glass.

The damage variable D can be determined from module measurements via eq.(1.1). The occurrence of this effect is in principle known from measurements on NaO-SiO_2 glass as the results by Ito and Tomozawa [4]. To the authors' knowledge, so far no measurements on fused silica are available. Therefore, we temporarily consider the damage D as a certain function of the hydroxyl concentration:

$$D = f(S) \tag{1.2}$$

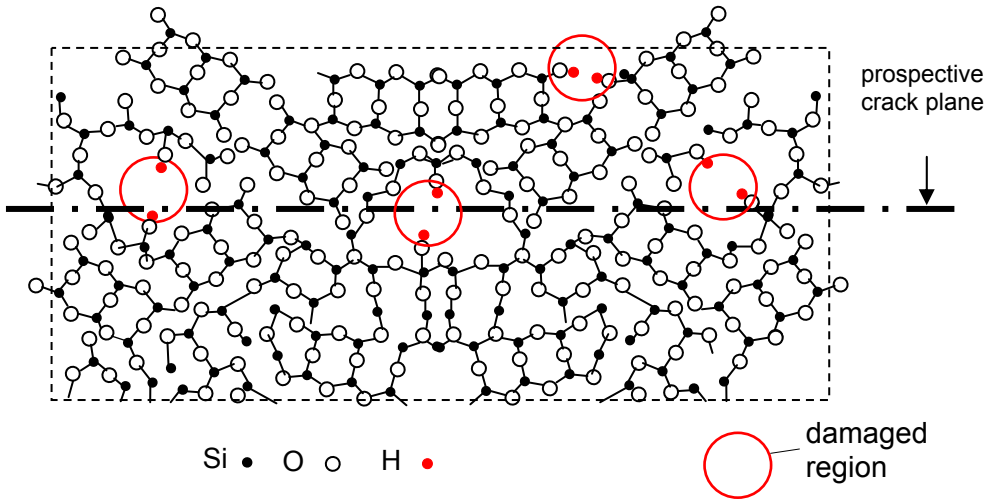

Fig. 1 Volume element of silica showing damage by bond breaking due to the water/silica reaction, third dimension ignored.

Apart from the equi-triaxial loading case with $\sigma_x = \sigma_y = \sigma_z$ (including the case of dis-appearing stresses), the elastic modulus must become a tensor with components depending on the degree of loading multiaxiality. Since this possibility would make the further treatment very difficult [3] and non-transparent, we assume in the following

considerations that the damage remains isotropic and is considered be of scalar nature. This is equivalent to the assumption of randomly orientated defects. Then also E remains isotropic. We assume that nano-pores in SiO_2, caused by hydroxyl generation, might behave like normal pores.

2 Experimental evidence for modulus reduction in silica

In literature, there is experimental evidence for modulus decrease with increasing hydroxyl content. This can be seen from measurements of Young's modulus as a function of water content. Measurements on longitudinal sound velocities in silica specimens with different water content were reported by Fraser [5] and Le Parc et al. [6]. Individual least-squares fits were made resulting for the data set by Fraser [5]

$$v \cong 5974\,(1-4.185S) \quad \text{in (m/s)} \tag{2.1}$$

and the set by LeParc et al. [6]

$$v \cong 5959(1-5.34S) \quad \text{in (m/s)} \tag{2.2}$$

When we normalize the results of the two test series on their individual values for S=0, we get the representation in Fig. 2. A common straight-line fit of these data yields

$$\frac{v}{v_0} = 1 - B\,S \tag{2.3}$$

with the parameter

$$B\text{=}5.04\ [4.23,\ 5.85]$$

(90%-CI in brackets).

The dependency of eq. (2.3) is introduced in Fig. 2 as the straight line. Since the longitudinal sound velocity depends on Young's modulus E and density ρ via $v \propto \sqrt{E/\rho}$, we obtain for small S with $\rho/\rho_0 \approx 1-(0.84/2)S$ according to the measurements by Shelby [7]:

$$\frac{E_D}{E_0} = \rho/\rho_0 \times (v/v_0)^2 = 1 - \lambda\,S \tag{2.4}$$

with λ=10.6 [8.7, 12.5]. It has to be noted that this value holds for isotropic damage since the natural OH-content doesn't show any preference for a special direction.

A comparable effect on E holds for porosity in ceramics. For hot-pressed silicon nitride (HPSN) with MgO and CeO_2 results over a much wider range of porosity were e.g. reported by Phani and Niyogi [8].

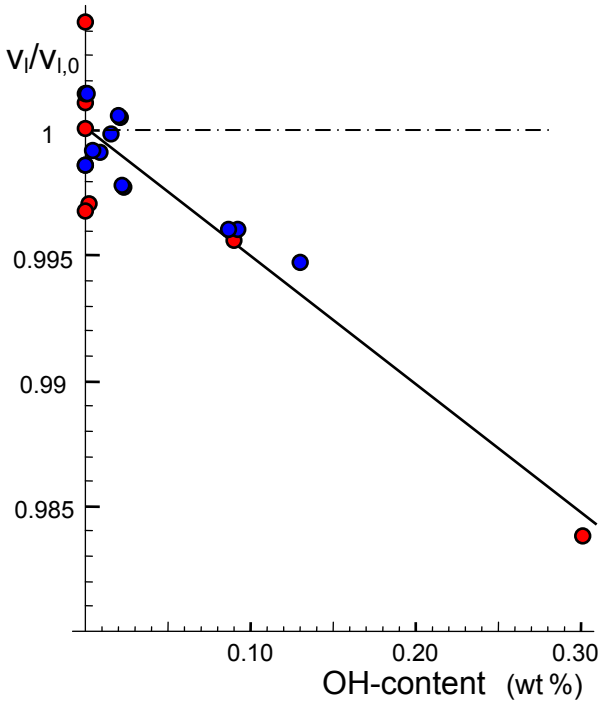

Fig. 2 Longitudinal sound velocity in silica with different OH-content (blue circles: results by Fraser [5], red circles: results by LeParc et al. [6]).

3 Modelling of damage by spherical pores

Analytical computations on the reduction of Young's modulus with porosity were carried out by Wang [9] for spherical pores. Unfortunately, the results were given as tabulated data. They were the basis of a number of fitting relations, mostly using exponential functions, which trivially must fail for large porosities since they could not represent the requirement of E=0 for a finite critical porosity. Wang [10] suggested a quadratic argument in the exponential function:

$$\frac{E_D}{E_0} = \exp[-A_1 P - A_2 P^2] \tag{3.1}$$

On the other hand, when P=1 (the whole volume is "pore") a finite modulus comes out what is of course not correct. An overview on descriptions can be obtained from [8-11].

Wang [9] determined the effect of porosity on Young' modulus theoretically via model computations. He changed the porosity by compacting a cubic array of spheres with identical size. Figure 3 illustrates ideal and nonideal cases of compaction (for details see [9]). The analytical data were given in a Table for three cases: the ideal case 1 in which each particle center remains on the lattice symmetry lines; case 2 for shear effects included and the case 3 for combined shear and hinge effects included.

The results of the computations are shown in Fig. 4a by the circles.

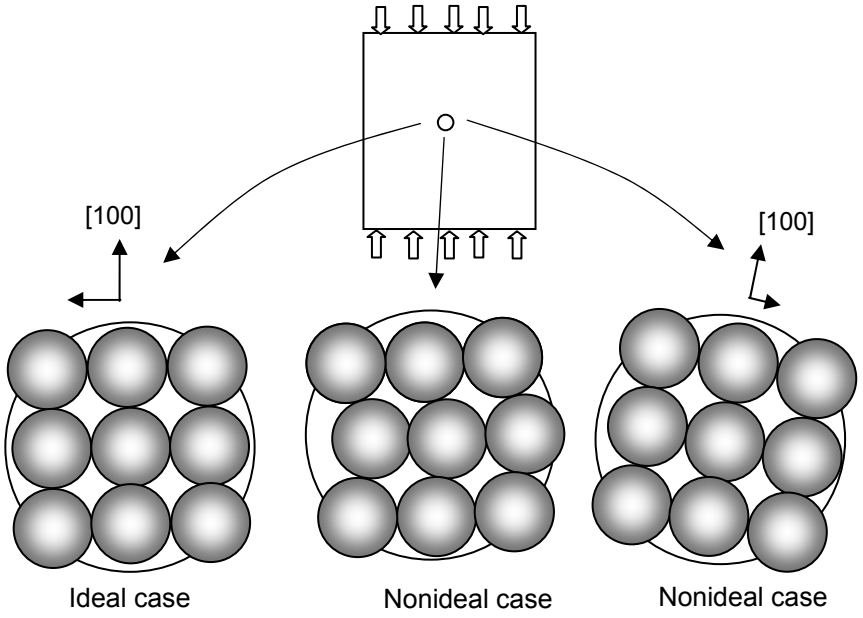

Fig. 3 Ideal and nonideal compacting by Wang [9].

We described the numerically given data by Wang [9] for all the three cases by the equation

$$\frac{E_D}{E_0} = \exp\left[- A_1 P - \frac{A_2}{(P_{\max} - P)^{1/n}} P^2 \right] \tag{3.2}$$

with $P_{\max}$=0.4764 from [9]. The other parameters A_1, A_2, and n were obtained by curve fitting to the numerical data.

The results are compiled in Table 1. The fitting curves are entered in Fig. 4. In order to show the good agreement of the fitting equation with the numerical data, the confidence intervals are given for case 3. The very narrow 90% confidence intervals indicate the good agreement with the numerical data.

Case	A_1	A_2	n
1	1.0286	1.6699	6
2	2.3289	2.6190	7
3	3.580 [3.565, 3.595]	3.747 [3.699, 3.795]	8

Table 1 Fitting parameters for eq.(3.2)

Figure 4b shows the numerical solution by Wang [9] as the circles and the linear dependency for small porosities

$$\frac{E_D}{E_0} \cong 1 - A_1 P \tag{3.3}$$

as the dashed straight line that intersects the abscissa at a characteristic porosity P_c of

$$P_c = 1/A_1 = 0.278\,P_{\max} \tag{3.4}$$

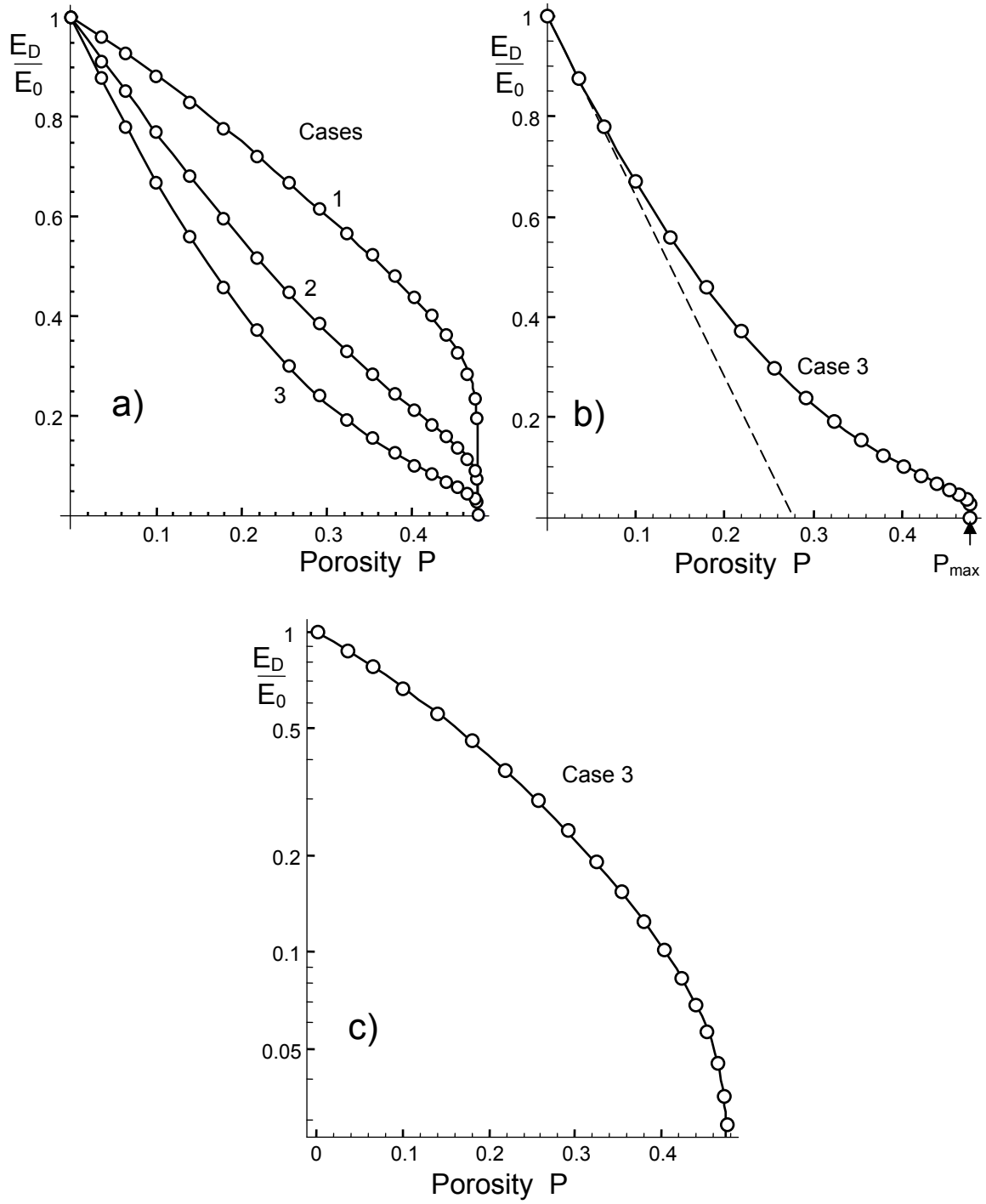

Fig. 4 Effect of porosity on Young's modulus for spherical pores; a) analytical results from Wang [9] (circles) compared with suggested fitting relation eq.(3.2) (curves); b) comparison of the approximation eq.(3.3) with (3.2), c) logarithmic ordinate scaling of the data in Fig. 4b.

The description by eq.(3.2) is entered as the solid curve. Good agreement between eq.(3.2) and the numerical data can be stated over the full porosity range.
In order to give a better resolution for the agreement at low modules, Fig. 4c represents the same results in logarithmic ordinate scaling.
For our purpose we rewrite eq.(3.2) by normalizing the porosities on the maximum value $P_{\max}$ and then replace P by S

$$\frac{E_D}{E_0} = \exp\left[-B_1 (S/S_{\max}) - \frac{B_2}{(1-S/S_{\max})^{1/8}} \left(\frac{S}{S_{\max}} \right)^2 \right] \tag{3.5}$$

with the parameters B_1=1.667, B_2=0.933. The result is plotted in Fig. 5 together with the linear approximation. From eq.(2.4) and the initial slope of eq.(3.5) we obtain via $B_1/S_{\max}=\lambda$ the maximum value of hydroxyl concentration

$$S_{\max} = \frac{B_1}{\lambda} = 0.157 \ \ [0.133, 0.192] \tag{3.6}$$

In [12] we derived from water concentrations on the surface of highly stressed cracks a hydroxyl concentration of

$$S = 16.5 \ [14.4, 18.4] \ \ (\text{wt\%}) \tag{3.7}$$

This result is in astonishing agreement with (3.6) with totally overlapping 90%-confidence intervals.

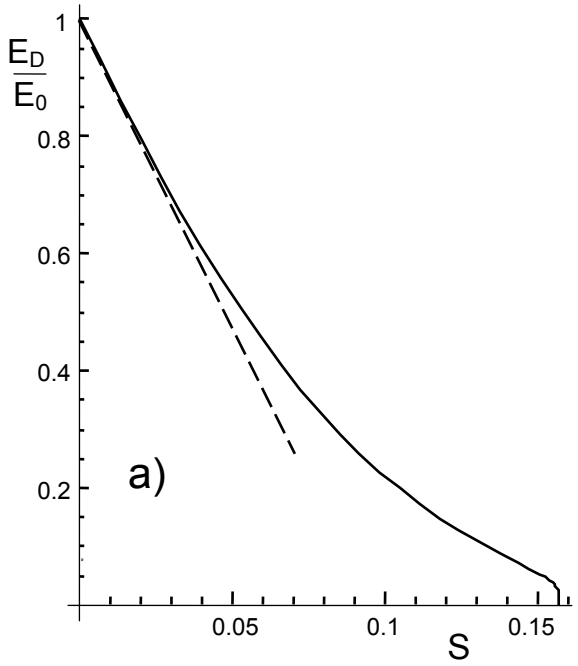

Fig. 5 Young's modulus as a function of hydroxyl concentration.

Here, it should be emphasized, that the theoretical result by Wang [9] is not necessarily an adequate description in other cases. Figure 6 shows results by Rice et al. [13] on reaction sintered silicon nitride (RSSN) which agree with the general trend of case 3 in Fig. 4 but showing finite modules even at porosities P>0.47. On the other hand there are measurements available for which the numerical results seem to be hardly applicable [8]. Such differences may come from the model assumptions: (I) ideal spherical particle shape, (II) regular particle and pore arrangement, (III) uniform size of the spheres. In real materials we have at least to expect particle- and pore-distributions and stochastically arranged particles.

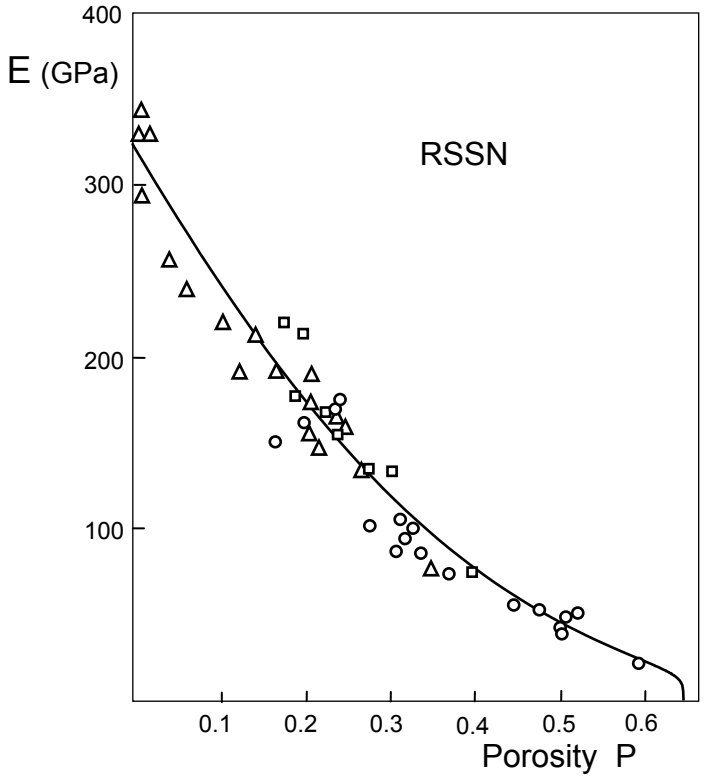

Fig. 6 Young's modulus for reaction sintered Si_3N_4 (RSSN) by Rice et al. [13] (circles), curve: eq.(3.5) for P_{max}≈0.65.

4 Effect of damage in thin surface layers

4.1 Global stress

If the damage is concentrated on thin surface layers of a thickness d that is small to the undamaged bulk thickness W, $d<<W$, the strain in the damaged surface layer must equal the strain in the bulk:

$$\varepsilon = \frac{\sigma_D}{E_D} = \frac{\sigma_0}{E_0} \tag{4.1}$$

The reduced average stress in the damaged surface, σ_D, is therefore according to eq.(1.1)

$$\sigma_D = \sigma_0 (1 - D) \tag{4.2}$$

(σ_0= stress in the undamaged bulk).
External loading in *z*-direction will increase the distance between atoms of the ring structure, resulting in the strain ε_z in loading direction. Failure of the material is reached, when the strain reaches a critical value ε_c. The damage in the material affects also the load-bearing capacity of any area element since it reduces its net cross section and, consequently, the strength of the damaged material σ_f. If $\sigma_{f,0}$ denotes the strength in the absence of damage, the strength of the damaged material is

$$\sigma_{f,D} = \sigma_{f,0} (1 - D) \tag{4.3}$$

The strength of water-damaged silica fibres is strain-controlled for $d << W$. This means that the strain at failure ε_c is the same in the surface layer and the bulk. This condition yields

$$\varepsilon_c = \frac{\sigma_{f,D}}{E_D} = \frac{\sigma_{f,0}(1 - D)}{E_0 (1 - D)} = \frac{\sigma_{f,0}}{E_0} \tag{4.4}$$

Equation (4.4) tells us that the damage problem can be handled simply by using bulk material parameters (E_0, $\sigma_{f,0}$) since the damage by broken bonds cancels out in (4.4).

4.2 Effect on crack resistance and stress intensity factors

The damage of the initial ring structure of silica, Fig. 1, must also affect the resistance against crack propagation. The crack growth resistance G_c represents the energy necessary to split all bonds that are broken when the crack has passed the considered volume element. Application of the damage variable yields for the crack growth resistance of the damaged material, $G_{c,D}$,

$$G_{c,D} = G_{c,0} (1 - D) \tag{4.5}$$

($G_{c,0}$ = crack resistance for the undamaged material, D=0) or in terms of stress intensity factors

$$K_{c,D} = \sqrt{E_D \, G_{c,D}} = K_{Ic} (1 - D) \tag{4.6}$$

where $K_{c,D}$ is the reduced toughness of the damaged material and K_{Ic} the fracture toughness measured in fracture mechanics tests on the undamaged material.

In the special case of a crack *fully embedded* in a material of reduced but constant modulus, E_D, the problem simplifies strongly. The applied stress intensity factor is generally given by

$$K_{appl} = \sigma_{appl} F \sqrt{\pi a} \tag{4.7}$$

(F = Fracture mechanics geometric function, a=crack length, Fig. 7).
Using the actual stress from eq.(4.2), K_{appl} reads for the crack fully embedded in the damaged zone

$$K_{appl,D} = \underbrace{\sigma_{appl,0} F \sqrt{\pi a}}_{K_{appl,0}} (1-D) = K_{appl,0}(1-D) \tag{4.8}$$

where $K_{appl,0}$ stands for the applied stress intensity factor formally computed with stresses σ_0 as present in the bulk material

$$K_{appl,0} = \sigma_0 F \sqrt{\pi a} \tag{4.9}$$

From (4.6), (4.8) and (4.9) it results equivalently to eq.(4.4)

$$\frac{K_{appl,D}}{K_{c,D}} = \frac{K_{appl,0}(1-D)}{K_{Ic}(1-D)} = \frac{K_{appl,0}}{K_{Ic}} \tag{4.10}$$

Also in terms of stress intensity factors, surface cracks fully embedded in the surface layer can be handled simply by using bulk material parameters (K_{appl}, K_{Ic}) instead of the unknown parameters in the layer.

4.3 Effect on pre-existing dimples

By removing the plastic protective coating on fibers with an acid, defects will be generated that can be described as hemispherical pits [14]. Depending on their geometry, such defects can reduce the surface strength clearly.
At the deepest point of a pit surrounded by the hydroxyl-damaged material under tensile stress σ_D, the stress is increased by the stress-concentration factor β, so that the maximum stress at the deepest point (A), Fig. 7, is

$$\sigma_{max,D} = \beta \sigma_D \tag{4.11a}$$

For a half-sphere it is for instance $\beta \approx 2$. Before the hydroxyl-damaged layer was generated, it did hold equivalently for the undamaged material under stress σ_0

$$\sigma_{max,0} = \beta \sigma_0 \tag{4.11b}$$

From eqs.(4.11a) and (4.11b) we have to conclude that in the case of failure the strengths in presence and absence of hydroxyl damage are reduced both by the common factor 1/β. When the strengths in presence of the pit are denoted by $\sigma_{f,pit,D}$ and $\sigma_{f,pit,0}$, it holds

$$\sigma_{f,pit,0} = \frac{1}{\beta}\sigma_{f,0} \tag{4.12a}$$

$$\sigma_{f,pit,D} = \frac{1}{\beta}\sigma_{f,D} \tag{4.12b}$$

Apart from the fact that the strength are reduced, it can be seen from the comined eqs. (4.12a) and (4.12b)

$$\frac{\sigma_{f,pit,D}}{\sigma_{f,D}} = \frac{\sigma_{f,pit,0}}{\sigma_{f,0}} \tag{4.13}$$

that also in this case the hydroxyl damage has no influence on strength.

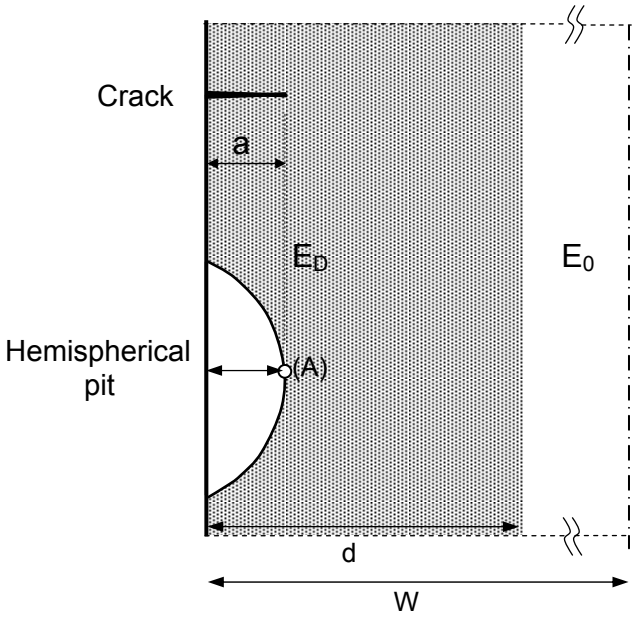

Fig. 7 Cross-section through a crack and a partially embedded hemispherical pit in a hydroxyl-damaged surface layer of thickness $d<<W$ (W= radius of the fiber) and $a<<d$.

4.4 Effect of swelling stresses

If the volume swelling occurs in a constrained manner, such as at the glass surface, then the swelling causes a build-up of compressive stresses in the surface region, which can strengthen the glass significantly as has been outlined in [15].

The compressive swelling stresses in axial and circumferential directions, y, z, respectively, are generally proportional to the product of volume swelling strain ε_v and Young's modulus E

$$\sigma_{sw,y}, \sigma_{sw,z} \propto \varepsilon_v E \tag{4.14}$$

For the most simple case of *isotropic* swelling, the proportional factor is for instance $1/(3(1-\nu))$, where ν is Poisson's ratio.
The related volume swelling strain, $\varepsilon_v > 0$, can be expressed by

$$\varepsilon_v = \kappa \times S \tag{4.15}$$

with the coefficient $\kappa \cong 0.97$.
When for example $\sigma_{sw,z,0}$ denotes the axial swelling stress in the undamaged material, it holds as a consequence of eq.(1.1) that the swelling stress in the hydroxyl-damaged surface is

$$\sigma_{sw,z,D} = \sigma_{sw,z,0}(1-D) \tag{4.16}$$

As an example, this dependency may be applied to the *crack-like surface defects*.
The so-called shielding stress intensity factor $K_{sh} < 0$ that shields the crack tip partially from the applied load is in the damaged material

$$K_{sh,D} = \sigma_{sw,z,D} F\sqrt{\pi a} = \sigma_{sw,z,0} F\sqrt{\pi a}\,(1-D) = K_{sh,0}(1-D) \tag{4.17}$$

where $K_{sh,0}$ stands for the shielding stress intensity factor in the undamaged material.
In presence of crack-tip shielding, failure occurs, when the total stress intensity factor K_{tip} reaches fracture toughness. In the damaged material the principle of superposition results in

$$K_{tip,D} = K_{appl,D} + K_{sh,D} = K_{Ic,D} \quad , \quad K_{sh,D} < 0 \tag{4.18}$$

Using eqs.(4.6), (4.8) and (4.17) gives the same result in terms of the stress intensity factors in the undamaged material

$$K_{tip,D} = (K_{appl,0} + K_{sh,0})(1-D) = K_{Ic,0}(1-D) \tag{4.19}$$

The equal sign on the right of (4.19) makes clear, that the shielding effect can be described by stress intensity factors in the undamaged material.

For the case of the surface additionally damaged by *pit-like surface defects*, the tensile stress σ_D, has to be replaced by the total stress $\sigma_D + \sigma_{sw,z,D}$ resulting equivalently to (4.19) in

$$\sigma_{\max,D} = \beta(\sigma_D + \sigma_{sw,z,D}) = \beta(\sigma_0 + \sigma_{sw,z,0})(1-D) = \sigma_{f,0}(1-D) \tag{4.20}$$

Again from the equal sign on the right, it becomes obvious that treatment with damaged quantities gives the same results as are obtained when hydroxyl damage is completely ignored.

5 Example of application: Uniaxial stress-strain curve

5.1 Swelling excluded

As has been outlined in [16], the hydroxyl concentration is stress-dependent. In order to allow a transparent derivation, swelling stresses may be neglected first. The hydroxyl concentration as a function of stress can be written

$$S = S_0 \exp[\gamma \sigma_{appl}] \tag{5.1}$$

At temperatures >500°C, the parameter γ reads for uniaxial loading [16]

$$\gamma = \frac{14.4(\mathrm{cm}^3/\mathrm{mol})}{RT} \tag{5.2}$$

The total strain ε under the applied stress σ is

$$\varepsilon = \frac{\sigma}{E_D(S)} \tag{5.3}$$

where for $E_D(S)$ or $D(S)$ the equation (3.5) has to be introduced.

The maximum stress, asymptotically reached for $\varepsilon \to \infty$, is

$$\sigma_{\max} = -\frac{1}{\gamma} \mathrm{Log}\left[\frac{S_0}{S_{\max}}\right] \tag{5.4}$$

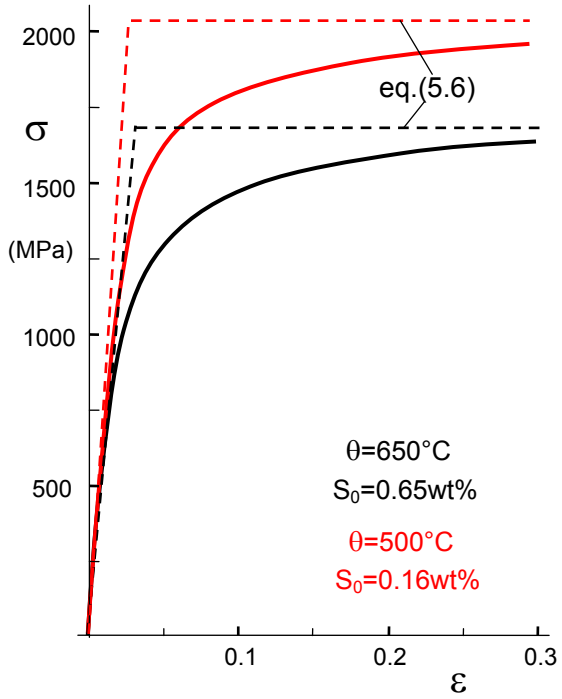

Fig. 8 Stress-strain curves, curve for 650°C and 500°C, hydroxyl concentrations S_0 from [16]; Approximate description of the stress-strain curves by eq.(5.6) (dashed lines).

In Fig. 8 the σ-ε-curves are shown for 650°C (355 Torr water vapour pressure) and 500°C with parameters S_0 (6 Torr pressure) taken from [16]. The dashed lines indicate the two asymptotes for $\varepsilon \to 0$ and $\varepsilon \to \infty$ of the solid curves.

For simpler mechanics computations, the stress-strain curves can be approximated by the two asymptotes (dashed lines in Fig. 8) where the rising part represents Young's modulus and the horizontal line the saturation stress given by eq.(5.4), i.e. a uniaxial "yield stress" $\sigma_Y = \sigma_{max}$. The initial Young's modulus E_{in} is slightly lower than the water-free module E_0 since already a hydroxyl concentration S_0 is present in the unloaded material

$$E_{in} \cong \left(1 - \frac{S_0}{S_{max} / A_1}\right) E_0 \cong E_0 \tag{5.5}$$

Then it holds

$$\sigma = \begin{cases} E_{in}\,\varepsilon & \text{for} \quad \varepsilon < \dfrac{\sigma_{max}}{E_{in}} \\ \sigma_Y & \text{for} \quad \varepsilon \geq \dfrac{\sigma_{max}}{E_{in}} \end{cases} \tag{5.6}$$

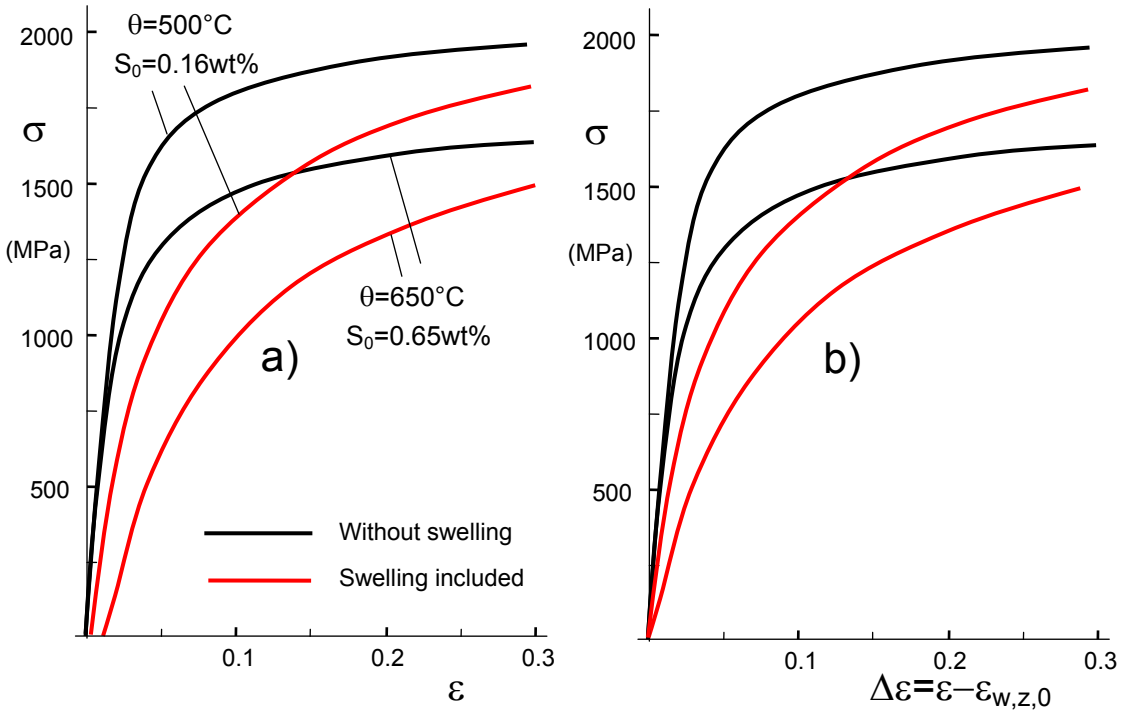

Fig. 9 Stress-strain curves, curve for 650°C and 500°C, black: without swelling, red: swelling included, a) total strain as the abscissa, b) strain by external loading as abscissa.

5.2 Swelling included

When swelling strains are taken into consideration, eq.(5.3) has to be replaced by

$$\varepsilon = \frac{\sigma}{E_D(S)} + \varepsilon_{sw,z} \tag{5.7}$$

where $\varepsilon_{sw,z}$ is the swelling strain in axial direction. According to [16] the eq.(5.1) yields

$$\varepsilon_{sw,z} = \alpha \kappa S = \alpha \kappa S_0 \exp[\gamma \sigma_{appl}] \tag{5.8}$$

with κ=0.97, α=1.92 [16]. The stress-strain curve obtained via eqs. (5.7) and (5.8) is shown in Fig. 9a as the red curves together with the curves by eq.(5.3) as the black ones. The offset of the red curves comes from the fact that even in the absence of stresses a swelling strain occurs that is caused by the initial hydroxyl concentration S_0. When $\varepsilon_{sw,z,0}$ is the swelling strain caused by the initial concentration S_0, the strain increase under load is $\Delta\varepsilon=\varepsilon-\varepsilon_{sw,z,0}$. This is shown in Fig. 9b.

6 Deviating behaviour under compressive loading

In the previous considerations we applied the model of pore-like defects. This model describes symmetrical material response under tension and compression loading. For special cases of applications the description by crack-like defects may be of advantage. This model allows introducing non-symmetry of deformation in tension and compression. Due to the fact that the crack surfaces cannot interpenetrate each other under compressive normal stress, the reduction of Young's modulus is less strong than in tension, represented by

$$E_D = \begin{cases} E_0(1-D) & \text{for} \quad \sigma \geq 0 \\ E_0(1-hD) & \text{for} \quad \sigma < 0 \end{cases} \tag{6.1}$$

with the crack closure parameter $0 \leq h \leq 1$, often found to be h=0.2 [17].

7 Effect of damage on crack-tip behaviour

7.1 Conclusions on the basis of the J-Integral

At crack tips under externally applied loads, the singular stresses must result in high hydroxyl concentrations and, consequently, high damage followed by a strong stress reduction. As long as a positive crack-tip stress intensity factor exists, $K_{tip} \geq 0$, also stress singularity must exist with $\sigma_{ij} \to \infty$. The hydroxyl concentration must reach its maximum possible value, S_{max}, with the consequence that the damage must tend to $D \to 1$ and the Young's modulus must disappear at the tip, $E_D \to 0$. These consequences

make the occurrence of singular stresses and a crack-tip stress intensity factor at least questionable.

The problem will be discussed here by using the path-independence of the J-Integral by Rice [18]. For any time-independent material behaviour the fracture mechanics J-integral can be used as the loading parameter. It simply reads for linear-elastic materials

$$J = \frac{K^2(1-\nu^2)}{E} = G \tag{7.1}$$

where the right-hand side is also called the energy release rate G. Since the J-integral for any path around the crack tip is a parameter independent of the specially chosen path, its value must be the same for a path Γ far away from the tip (in the bulk) and the path Γ_D directly at the crack tip, i.e. in the damaged region as is illustrated in Fig. 10

$$\frac{K_{appl}^2(1-\nu_0^2)}{E_0} = \frac{K_{tip}^2(1-\nu_D^2)}{E_D} \tag{7.2a}$$

where E_D and ν_D are the elastic properties at the tip affected by water. For $\nu_D \cong \nu_0$

$$K_{tip} \cong K_{appl}\sqrt{\frac{E_D}{E_0}} \tag{7.2b}$$

This relation also holds for notches [19].

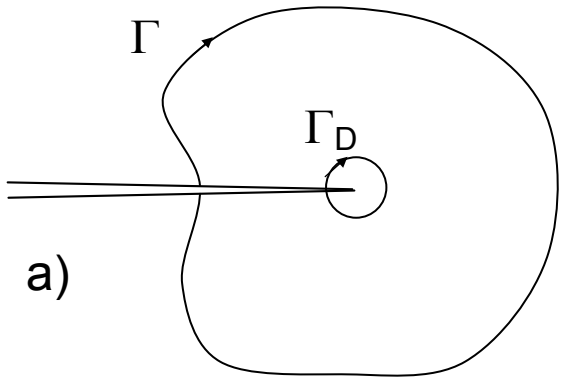

Fig. 10 Two J-integral paths around a crack tip; path Γ far away from the tip reflects the properties of the bulk material, path Γ_D the water-affected and damaged crack-tip region.

<u>*Conclusion*</u>: Since in eq.(7.2a) a finite value on the left-hand side is prescribed by the external loading, the right-hand side must be finite, too. For the crack tip it results due to $\sigma_{ij} \to \infty$ that: $S \to S_{max}$ and $E_D \to 0$. The disappearing denominator E_D requires that also the numerator must disappear. Consequently, it must hold $K_{tip}=0$ resulting in finite stresses.

7.2 Description by plastic-zone models

Due to the damage via hydroxyl generation, the stress-strain behavior at a crack tip is no longer linear. By application of the eqs.(5.1) and (5.4), fracture mechanics problems can be easily solved applying the well-known Irwin [20] and Dugdale [21] models, originally developed for elastic/plastic material behaviour. Whereas the Irwin model is preferred for circular "plastic zones", the Dugdale model describes plastic deformations in a narrow strip in front of the crack.
According to these models the "length" of the "plastic" zone, (Fig. 11), is

$$L_{Irwin} = \frac{1}{\pi}\left(\frac{K_{appl}}{\sigma_Y}\right)^2 \tag{7.3a}$$

for the Irwin model and

$$L_{Dugdale} = \frac{\pi}{8}\left(\frac{K_{appl}}{\sigma_Y}\right)^2 \tag{7.3b}$$

for the Dugdale model. σ_Y is the yield or flow stress given by $\sigma_Y=\sigma_{max}$ of eq.(5.4). Both models show nearly the same results.

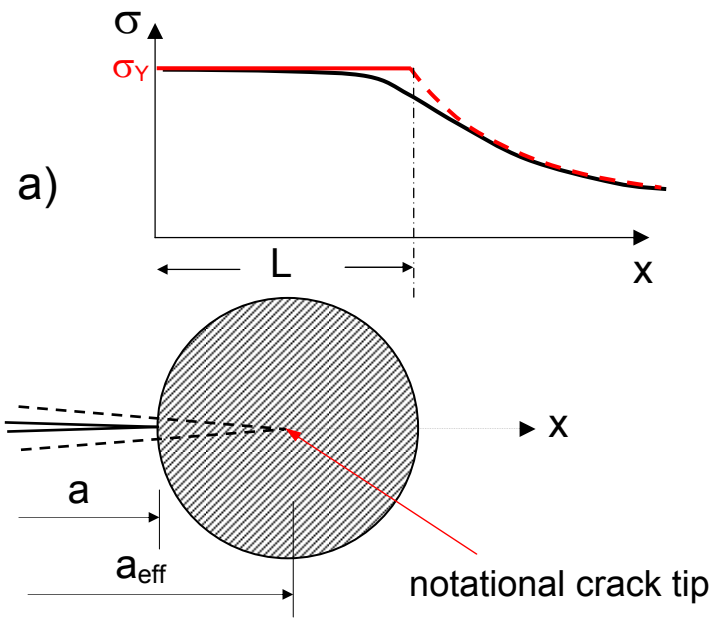

Fig. 11 Stress distribution curve near a crack tip (black curve) approximated by an elastic-"plastic" model.

Further consequences of the disappearing stress singularity at crack tips will be studied in a separate report.

References

1 L.M. Kachanov, Time of the rupture process under creep conditions, TVZ Akad Nauk S.S.R. Otd Tech. Nauk **8**(1958)

2 J. Lemaitre, Evaluation of dissipation and damage in metals, Proc. I.C.M. 1, Kyoto Japan (1971).

3 J. Lemaitre, How to use damage mechanics, Nuclear Engng. Design **80**(1984), 233-245.

4 S. Ito and M. Tomozawa, J. de Phys. C9 (1982), 68.

5 D.B. Fraser, Factors Influencing the Acoustic Properties of Vitreous Silica, Citation: Journal of Applied Physics 39(1968), 5868-5878.

6 R Le Parc, C Levelut, J Pelous, V Martinez, B Champagnon, Influence of fictive temperature and composition of silica glass on anomalous elastic behavior *J. Phys.: Condens.* Matter **18**(2006), 7507-27.

7 Shelby, J.E., "Density of vitreous silica," J. Non-Cryst. **349** (2004), 331-336.

8 Phani, K.H., Niyogi, S.K., Elastic-modulus–porosity relationship for Si_3N_4, J. Mater. Sci. Letters **6**(1987), 511–515.

9 J.C. Wang, Young's modulus of porous materials, Part 1, J. Mater. Sci. **19**(1984), 801-808.

10 Wang, J.C., Young's modulus of porous materials, Part 2, *J Mater Sci*. 1984;19:809-814.

11 Phani, K.H. Niyogi, K. De, Porosity dependence of fracture mechanical properties of reaction sintered Si_3N_4, J. Mater. Sci. Letters **7**(1988), 1253–1256.

12 T. Fett, G. Schell, Damage in silica by hydroxyl damage, Scientific Working Papers, SWP **85**, 2018, KIT Scientific Publishing, Karlsruhe.

13 R.W. Rice, K.R. McKinney, C.M. Wu, S.W. Freiman, W.J.M. Donough, J. Mater. Sci. **20**(1985), 1392.

14 D. Inniss, Q. Zhong, C.R. Kurkjian, Chemically corroded pristine silica fibers: Blunt or sharp flaws?, J. Am. Ceram. Soc. **76**(1993), 3173-77.

15 S.M. Wiederhorn, T. Fett, G. Rizzi, M. Hoffmann, J.-P. Guin, "Water Penetration – its Effect on the Strength and Toughness of Silica Glass," *Met. Mater. Trans. A*, **44** [3], 1164 - 1174 (2013).

16 S. M. Wiederhorn, G. Rizzi, S. Wagner, M. J. Hoffmann, and T. Fett, Stress-Enhanced Swelling of Silica: Effect on Strength, J. Am. Ceram. Soc. **99**(2016), 2956-63.

17 J. Lemaitre, J.P. Sermage, One damage law for different mechanisms, Comp. Mech., **20**(1997), 84-88.

18 Rice, J.R., A path independent integral and the approximate analysis of strain concentration by notches and cracks, Trans. ASME, J. Appl. Mech. (1986), 379-386.

19 J. G. Merkle, An application of the J-integral to an incremental analysis of blunt crack behavior, Mechanical Engineering. Publications, London, 1991, 319-332.

20 G.R. Irwin, Plastic zone near a crack and fracture toughness. Proc. 7th Sagamore Ordnance Res. Conf. Racquette Lake NY, August 16-19, pp. 63-78.

21 Dugdale, D.S., "Yielding of steel sheets containing slits", *J. Appl. Mech. Solids* **8**(1960), 100-104.

KIT Scientific Working Papers
ISSN 2194-1629

www.kit.edu